

Motility-sorting of self-propelled particles in micro-channels

ANDREA COSTANZO, JENS ELGETI, THORSTEN AUTH, GERHARD GOMPPER AND MARISOL RIPOLL

*Theoretical Soft Matter and Biophysics, Institute of Complex Systems
Forschungszentrum Jülich GmbH, D-52425 Jülich, Germany*

PACS 64.75.Gh – Phase separation and segregation in model systems

PACS 87.10.Mn – Stochastic modeling

PACS 05.65.+b – Self-organized systems

Abstract – Spontaneous segregation of run-and-tumble particles with different velocities in microchannels is investigated by numerical simulations. Self-propelled particles are known to accumulate in the proximity of walls. Here we show how fast particles expel slower ones from the wall leading to a segregated state. The mechanism is understood as a function of particle velocities, particle density, or channel width. In the presence of an external fluid flow, particles with two different velocities segregate due to their different particle fluxes. Promising applications can be found in the development of microfluidic lab-on-a-chip devices for sorting of particles with different motilities.

Introduction. - Self-propelled particles are small biological or synthetic systems that transform energy into directed motion [1]. Microorganisms like bacteria, sperm cells or other eukaryotic cells, as well as synthetic particles like nanorods or Janus colloids, employ various strategies to generate directed motion in a fluid environment [2,3]. Ensembles of self-propelled particles can form clusters [4–11] and concentrate in space regions delimited by walls of funnels [12,13]. Furthermore, active particles have been shown to accumulate in the proximity of the walls [14–16], resulting for example in trapping of particles in microwedges [17,18], spiral vortex formation in circular confinement [19], or depletion of elongated particles from low-shear regions [20]. Further interesting phenomena, which are only possible with active particles, are the upstream swimming in microchannels with capillary flow [21–24], spontaneous directed rotation of asymmetric wheels [25–27], or net particle flux in static potentials [28–30].

Populations of active particles in nature frequently have a wide distribution of certain properties. For example, sperm cells have a range of velocities, and only a few of them are able to reach the ovum and fertilize it; Janus colloids have a range of sizes and chemical activity. Nature has developed strategies to sort particles with certain properties depending on their functionality. Sorting strategies are also interesting in technological applications for self-propelled particles. Thus, a deeper understanding of sorting mechanisms is of great fundamental and

technological importance, which has already originated numerous studies. The famous Maxwell’s demon is able to separate fast and slow gas molecules, unfortunately by violating the second law of thermodynamics. At the macroscopic scale, several studies focused on the problem of sorting particles, exploiting entropic means [31], gravity [32], and microfluidic devices [33–37]. At the microscopic scale, spontaneous segregation of active and passive particles, freely swimming in a two-dimensional box with periodic boundary conditions, has been numerically investigated [38]. Separation of self-propelled particles with different motilities have been investigated for asymmetric obstacles [39] and using centrifuges [40].

In this work, we investigate numerically how the accumulation of self-propelled particles at walls can be exploited to sort particles with different velocities. Accumulation of faster particles in the proximity of the walls is characterized for microchannels as a function of particle velocities, channel width, and particle concentration. In the presence of a capillary flow, it is shown that the downstream flux is enriched with the slower self-propelled particles. The combination of a capillary flow with membranes shows accumulation at both channel ends, with the downstream end enriched in slow particles, and the upstream end populated almost exclusively by fast particles. Potential applications in fields as diverse as microfluidics, biology or even reproductive techniques motivate our study.

Model. - We employ a minimal model for self-propelling run-and-tumble bacteria [21], aimed at mimick-

ing the motion of *E. coli* [41]. Each particle is described by two beads of diameter a rigidly connected at distance a , such that the length of the particle is $l = 2a$. During the run time, the particle center of mass is subjected to a force directed along its main axis, which determines the self-propulsion velocity v via its friction coefficient in the fluid. The stochastic tumbling event interrupts the run at random times with constant rate and duration, by imposing a random torque on the particle which lets a free particle rotate by a random angle uniformly distributed in $(0, 2\pi)$. We take the duration of the tumbling τ as time unit. Distances are measured in units of the particle length l , such that for example velocities are given in units of l/τ . The average time between tumbling events is chosen to be 10τ and the average free-run-length is $\lambda = 10l$. Previous work with this model [21], as well as other recent experimental [9, 42] and simulation [14, 15] studies, indicate that the role of hydrodynamic interactions in wall or cluster aggregation is often negligible in comparison with steric interactions, especially for elongated particles. Hydrodynamic interactions are therefore disregarded here. Equations of motion are integrated with the second order Runge-Kutta method with time step $\Delta t = 10^{-3}$. The chosen tumbling parameters determine the value of the single particle rotational diffusion to be $D_r = 0.3$. We employ velocities between 0 and 2, such that $Pe = v/(lD_r) = 6.6$ is the maximum value of the Peclet number. We consider N particles in a box with dimensions L_x and L_y , with periodic boundary conditions in the y -direction, and confining walls in the x -direction. Short-range soft repulsive interactions ($V(r) \sim r^{-12}$, with cut-off radius $r_c = 3$) are considered between the beads, and also between the beads and the walls. The number density is $\rho = N/A$ with A the box area. As a reference, the density of hexagonally packed impenetrable beads of diameter a is $\rho_m \simeq 2.31$.

We investigate one-component reference systems, in which all particles have the same self-propulsion velocity v , and equimolar two-component systems, in which half the particles have velocity v_f and the other half velocity v_s , with $v_f > v_s$, and with an average velocity $\bar{v} = (v_f + v_s)/2$. Standard parameters $L_y = 20$, $L_x = 10$, $\rho = 1$, and $\bar{v} = 1$ are employed unless otherwise stated. Starting from random initial configurations, we typically compute time averages over 10^6 time steps (corresponding to an average of 100 tumbling events for a single free particle) excluding the initial 10^5 for equilibration, and consider 8 independent runs to average physical quantities of interest.

Particle mixtures in confinement. - First, we investigate the properties of self-propelled particles confined in a microchannel, with walls in the x -direction and periodic boundary conditions in the y -direction. We are interested in characterizing the density of particles across the channel width. We define $\rho^\alpha(x)$ as the local number density of the particles centers of mass, with α denoting the considered species. In fig. 1, average normalized density profiles are displayed for two one-component systems with velocities $v = 0.5$ and $v = 2$. Increasing particle velocity enhances

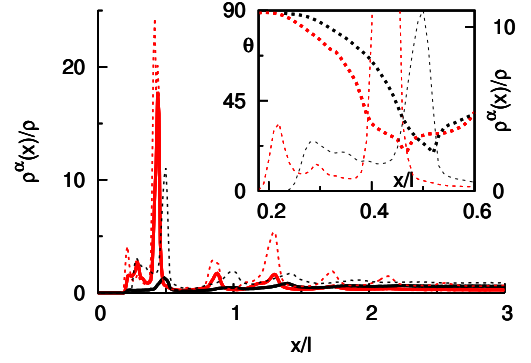


Fig. 1: (Color online) Normalized local number density of the particles centers of mass $\rho^\alpha(x)$ in a microchannel as function of the wall distance. Two independent one-component systems are displayed with dashed lines, and the two components of an equimolar mixture are shown with solid lines. Black denotes $v = 0.5$ and red $v = 2$. Inset: magnification of the region close to the wall. Additional thick-dotted lines are the angle of particles with the wall normal vector for the one-component systems.

the accumulation of particles at the wall (higher values of the ρ^α maximum peaks). The averaged orientation of particles with the wall normal vector, θ , is shown in the inset of fig. 1. Motility does not significantly change θ . The slight peak offset in the density profiles is then exclusively due to the softness of the interaction potentials. As a consequence of the wall accumulation, the density in the bulk decreases with v . Figure 1 also shows the density profiles of each of the two components in a mixture. The density peak of slow particles next to the walls is clearly suppressed in the mixture. This happens via an *expulsion mechanism*, as shown in fig. 2b. When particles at the wall happen to be in a configuration in which they are pushed symmetrically from both sides, slow particles are expelled into the bulk. Therefore, fast particles are more abundant close to the walls, and slower particles in the bulk, as can be seen in fig. 2a.

In order to characterize the segregation of both components, we define the separation parameter as

$$\psi^\alpha = \frac{\int_0^d \rho^\alpha(x) dx}{\sum_\alpha \int_0^d \rho^\alpha(x) dx}. \quad (1)$$

This quantity measures the percentage of one species in the particle population found close to the wall, indicating its relative accumulation. We employ $d = l$, the particle length, to analyze separation. Other distances, larger, but considerably smaller than $L_x/2$ would provide qualitatively similar results. By construction, $\psi^\alpha = 1$ or $\psi^\alpha = 0$ for complete separation, while for completely mixed two-component system $\psi^\alpha = 0.5$.

In fig. 3, we analyze the dependence of the separation as a function of the difference of velocities $\Delta v = v_f - v_s$, average velocity \bar{v} , density ρ , and channel width L_x . In-

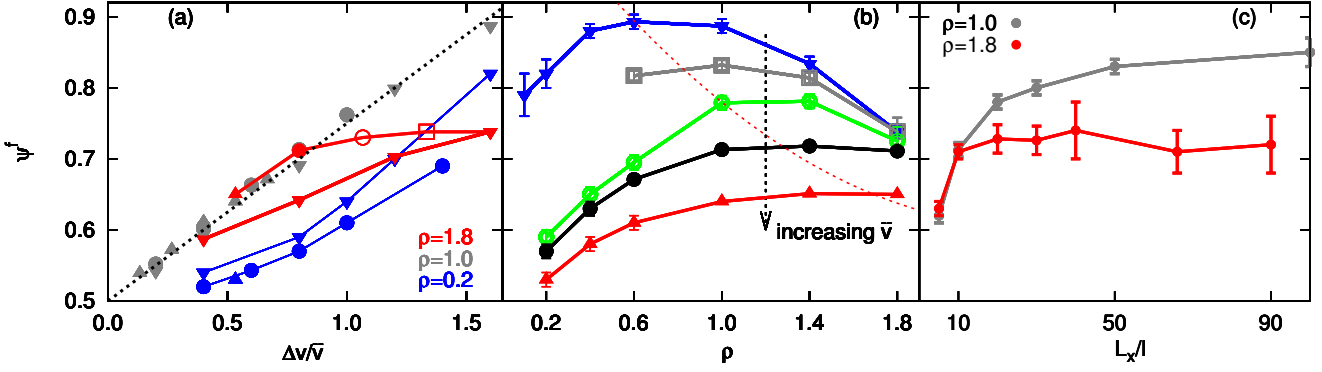


Fig. 3: (Color online) Fraction of fast particles close to the wall, quantified by ψ^α in Eq. (1). Besides standard parameters, in (b) and (c)

$\Delta v = 0.8$. Dependence on (a) normalized velocity difference (b) density, and (c) system size. In (a) and (b) symbols consistently denote values of \bar{v} : $\bar{v} = 0.5$ (\blacktriangledown), $\bar{v} = 0.6$ (\square), $\bar{v} = 0.75$ (\circ), $\bar{v} = 1.0$ (\bullet), $\bar{v} = 1.5$ (\blacktriangle). The dashed line in (a) is the linear interpolation $\psi^f = 0.25\Delta v/\bar{v} + 0.5$ and other lines are guides to the eye.

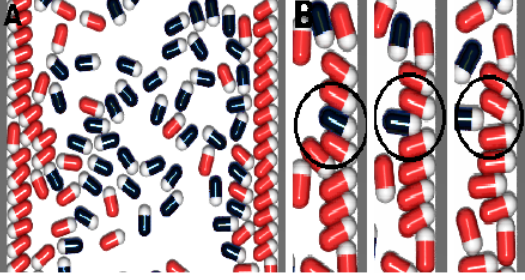


Fig. 2: (Color online) Simulation snapshots of a mixture of slow ($v_s = 0.6$, black) and fast particles ($v_f = 1.4$, red). (a) Fast particles accumulate at the walls, while the slow ones are displaced into the bulk. (b) One slow particle is being *expelled* away from the wall. See also `movie1.avi`.

creasing Δv naturally leads to a larger separation. This dependence can be understood better by normalizing Δv by \bar{v} , as shown in fig. 3a. Complete separation, $\psi^f = 1.0$, is expected for a mixture with one passive component, where $\Delta v = 2\bar{v}$, while for a system with equal velocities $\psi^f = 0.5$. A linear interpolation between both limits is then a reasonable first guess, and it shows indeed to be a very good approximation for the behaviour of systems with intermediate densities. For small densities, the accumulation at the walls is also small. The encounters of a larger number of particles at the walls is not frequent enough for the expulsion mechanism to be effective, therefore the separation is less efficient. For high densities, the accumulation at the wall is much higher. Situations with more than one layer of particles at the wall are frequent, resulting in a hampering of the expulsion mechanism. Interestingly, curves for different average velocity seem to approach nearly the same value of the separation parameter, $\psi \simeq 0.75$, for high densities. A continuous crossover between the behavior at small and large particle densities can be observed in fig. 3b. The separation as a function

of ρ displays a local maximum for smaller values of the average velocity \bar{v} , but it is monotonically increasing with ρ for larger \bar{v} . The density that optimizes the separation increases with increasing \bar{v} (dashed red curve in fig. 3b). At constant Δv and ρ , separation decreases with increasing \bar{v} , as shown in fig. 3a and b. This happens because $\Delta v/\bar{v}$ is the relevant quantity to consider, as already mentioned above. An absolute velocity difference Δv is less relevant when the two velocities are high, compared to the situation when the two velocities are low.

The channel width might also influence the separation of the two components. When the channel is wide enough, the accumulation at each wall can be understood independently of the presence of the other wall. This is not the case for narrow channels, where particles expelled from one wall very soon arrive at the second wall, hindering separation. In fig. 3c, the separation is shown as function of the channel width L_x . The transition from weak to strong confinement varies with density and with the average free-run-length λ . At standard density $\rho = 1$, we observe a monotonic increase of the separation, reaching a plateau value at $L_x > 5\lambda$. At high density $\rho = 1.8$, the plateau value is reached already in smaller channels $L_x \simeq \lambda$. Other factors that influence component separation, like the particle aspect ratio or swimming strategy, will be a matter of further investigation.

Particle mixtures in a capillary flow. - Flow through microfluidic devices presents a unique possibility to study and manipulate microswimmers. We modify our simulation model to include the effect of an implicit fluid with a parabolic velocity profile, with maximum velocity v_0 at the center of the channel and vanishing flow velocity at the walls. This is performed by adding to the translational and rotational velocities of each particle both the velocity and the vorticity of the flow [21].

In the absence of flow, particles accumulate at the wall with a certain orientation, but always symmetric on aver-

age with respect to the surface normal vector [15, 21]. In the presence of flow, the interplay of self-propulsion and the vorticity field of the flow implies that the orientation of particles accumulated at the wall is almost exclusively opposite to the applied flow (see fig. 4 and *movie2.avi*). This gives rise to the interesting phenomenon of *upstream swimming* at the channel walls. This affects the entire velocity profile of the particles across the whole channel. For a given flow field, upstream swimming increases with self-propelling velocity. Furthermore, the trajectories of single self-propelled non-tumbling particles in a parabolic flow also result in an upstream average orientation, which enhances the upstream swimming [21–24]. On the other hand, tumbling and collisions among particles randomize the particle orientation, such that the particle average velocity follows more easily the applied flow. Interestingly, the velocity at the channel center v_c can become larger than the applied flow v_0 , see fig. 4. This means that the particles are on average aligned with the flow, in contrast to the previously described effects. This effect occurs for not too small densities, moderate self-propulsion velocities, and it is most likely related to a cooperative phenomenon. The combination of these effects can result in the non-monotonic dependence of the velocity at the channel center v_c with the self-propelling velocity, as shown in fig 4b, where the increase of v_c with density is also displayed.

The question that arises now is how the presence of flow affects the spontaneous separation in mixtures of self-propelled particles with different velocities. The local particle density $\rho^\alpha(x)$, shown in fig. 4, indicates that the fast particles still expel the slow ones from the near-wall region into the bulk, and that the presence of flow slightly diminishes layer formation in the proximity of the walls, similar to the one-component case [21]. The velocity profiles of each component $v_y^\alpha(x)$ are displayed in fig. 4. Both profiles differ from their counterparts in the one-component systems by getting closer to each other, which reflects the effective drag of one particle component on the other.

In order to quantify the separation of components in the presence of flow, we compute the particle flux ϕ^α of each component, which is defined as

$$\phi^\alpha = \int_0^{L_x} \rho^\alpha(x) v_y^\alpha(x) dx. \quad (2)$$

This quantity expresses the number of particles crossing a channel section in a unit of time, and its value is a consequence of the interplay of density and velocity profiles. In the case of passive tracer particles with a flat density profile moving in a parabolic flow with maximum velocity v_0 , the flux can be calculated easily to be $\phi_0 = 2\rho v_0 L_x/3$. In fig. 5, the normalized flux ϕ/ϕ_0 is displayed for various one-component systems as a function of v . The limit of passive particles $\phi \rightarrow \phi_0$ is reasonably well reproduced, given that the density profile is never perfectly flat in the presence of confining walls. With increasing self-propulsion velocity, the flux decreases as a consequence

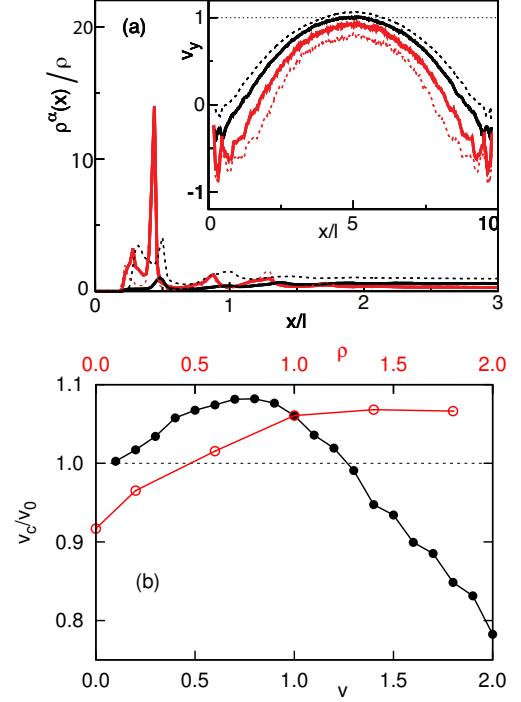


Fig. 4: (Color online) (a) Normalized local number density of the particles centers of mass in the presence of a capillary flow with $v_0 = 1$. Inset: velocity profiles along the channel width. Axis, lines, and parameters as in fig. 1. (b) Average velocity at the center of the channel v_c as a function of particle density (circles) and particle self-propulsion velocity (bullets).

of the increase of the upstream swimming. In general, however, the dependence of the normalized flux on other system parameters is non-trivial. Increasing the average density shows a non-monotonic albeit very small variation of the normalized flux. Increasing the fluid velocity increases the normalized flux, which indicates that the particles follow the flow more the stronger it is, which is also the effect of enlarging the channel width.

In a mixture, the changes in the velocity profiles translate into a slight increase of the fast-particle flux relative to the single-component case, while for slow particles the flux slightly decreases. This is shown in the inset of fig. 5, where the one-component reference normalized flux is compared with the values for each of the mixed components. Only for $\bar{v} = 0.5$, we observe a slight flux increase for both components. In this case, the interplay between density and velocity is different, and the separation is more effective.

The separation of fast and slow particles obtained in the outflow can be characterized by the difference of the fluxes of both components $\Delta\phi = \phi^s - \phi^f$. This difference increases with density, fluid velocity, and channel width, similar to the normalizing flux ϕ_0 , and naturally also with the difference of velocities, as displayed in the inset of fig. 6. Figure 6 shows that the largest normalized flux differences occur for the smallest employed flow veloc-

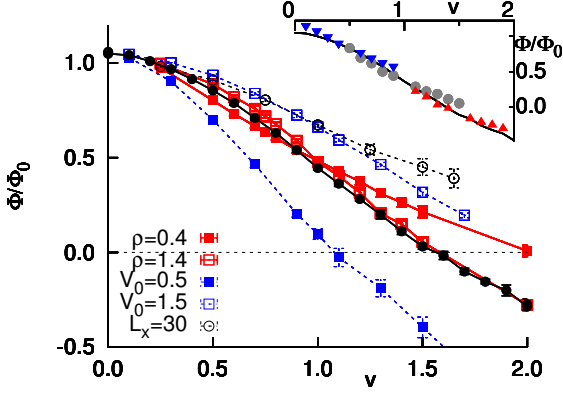


Fig. 5: (Color online) Normalized flux of one-component systems as a function of the self-propulsion velocity. Labels indicate non-standard parameters. Inset: the line corresponds to the one-component reference flux, and symbols to the mixture components. Four mixtures with different Δv are displayed for each \bar{v} . Symbols indicate $\bar{v} = 1.5$ (\blacktriangle), $\bar{v} = 1.0$ (\bullet), and $\bar{v} = 0.5$ (\blacktriangledown). Fluxes are normalized such that $\Delta v \rightarrow 0 \Rightarrow \phi^\alpha \rightarrow \phi$.

ity. At that flow velocity the single-component normalized flux shows the largest decrease with self-propulsion velocity (fig. 5). As we have shown above, the mixing only slightly changes the flux values, such that the behavior of the single-component fluxes can be taken as a reference for flux differences in mixtures. An interesting consequence arising from the flux presented in fig. 5 is that for a given mixture, the applied flow velocity can be eventually tuned to obtain a positive flux for the slow particles and a negative flux for the fast particles. For example, this can be achieved for a mixture with $v_s = 0.5$ and $v_f = 1.5$ and standard parameters by choosing $v_0 = 0.5$.

Particles mixtures in microchannel flow confined between membranes. - An interesting configuration to exploit the separation of self-propelled particles of different self-propulsion velocities in microcapillary flow is shown in fig. 7a. It consists of two semi-permeable membranes spanned across the channel diameter at a defined channel segment. The membrane pores are assumed to be too small for the particles to penetrate, but large enough for the fluid flow to pass unhindered. Thus, in our simulations, the fluid flow is unperturbed compared to the open channel, while excluded-volume interactions are implemented for the self-propelled particles.

At the walls, the particles mostly move fast and upstream, which in the presence of the membranes leads to the accumulation of almost exclusively fast particles at the upstream membrane, as shown in fig. 7a and in *movie3.avi*. In the center of the channel, equidistant from the walls, both particle types are present and move downstream, but slow particles are more abundant. This leads to an accumulation of a mixture of particles that is enriched in slow particles at the downstream membrane. The competition of these two effects determines the precise distribution of particles along the channel, which therefore

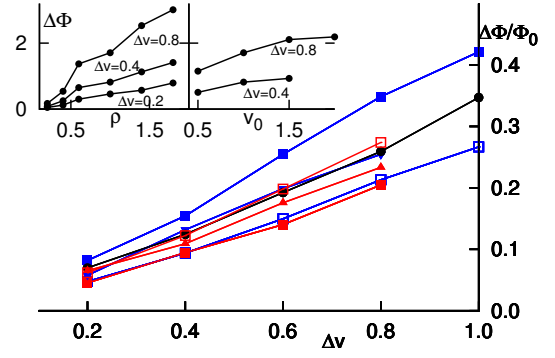


Fig. 6: (Color online) Normalized flux difference for two-component systems, as a function of Δv . Inset: flux difference as a function of density and fluid velocity. Symbols are the same as in fig. 5.

strongly depends on the system parameters. The intrinsic distribution of self-propelled particles in the channel also translates in the accumulation at the membranes, which is much more ordered upstream than downstream.

In order to quantify the separation, we compute the percentage of fast particles at a distance d from the upstream-membrane, ψ_u^f , and the percentage of slow particles at a distance d from the downstream-membrane, ψ_d^s , which is calculated using Eq. (1) with $d = L_y/4$. Relevant quantities are also the total particle densities ρ_u and ρ_d in both regions. The dependence of the separation parameters and densities close to the membranes on the applied flow velocity is presented in fig. 7b for a mixture with $v_s = 0.5$ and $v_f = 1.5$. In the absence of flow, there is no separation, $\psi^\alpha = 0.5$, and both densities are equal to $\rho = N/A$, which in this case is 1.25. By increasing the fluid velocity, the particles are increasingly pushed to accumulate at the downstream membrane, reaching a packing limit where neighboring particles can be slightly closer than the bead diameter due to the soft interaction potential. Interestingly, only fast particles are found at the upstream membrane for $v_0 \geq v_s$, while the largest proportion of slow particles is found at the downstream membrane for flow velocities a bit larger than v_s .

Conclusions. - The separation of run-and-tumble particles in terms of their motility in a microchannel has been studied. Slow particles are shown to be *expelled* by the fast neighboring particles from the wall into the bulk, which results in the spontaneous segregation of the two components. This mechanism can be of importance to achieve particle sorting, *e.g.*, via a pipette or a microfluidic device. We have also investigated how the presence of a capillary flow in the microchannels affects segregation. In this case, since particles with different velocities have different fluxes, the fluid velocity can be tuned to segregate slow particles downstream and fast particles upstream. Separation always grows with the velocity difference, but the dependence on other parameters is less obvious. In the

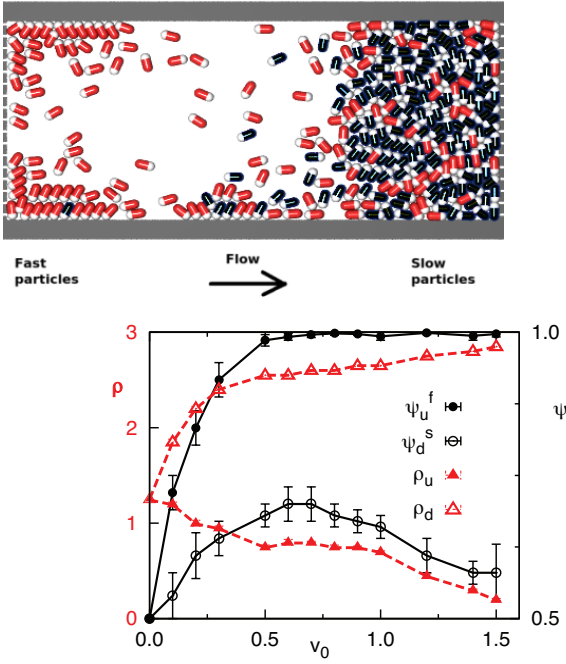


Fig. 7: (Color online) (a) Simulation snapshot of a micro-channel with capillary flow ($v_0 = 1.0$) and confining membranes. Fast particles ($v_f = 1.5$) are found upstream and slow ones ($v_s = 0.5$) downstream. (b) Percentage of fast particles in the upstream quarter of the channel ψ_u^f , and of slow particles in the downstream quarter ψ_d^s as a function of v_0 . Total number densities in each quarters, ρ_u and ρ_d .

absence of flow, separation is maximized for low average particle velocities and intermediate densities. In the presence of flow, separation grows with fluid velocity, channel width, and density, while there is almost no dependence on the average particle velocity. Moreover, the separation of fast and slow particles in a channel with flow and membranes at its ends has shown to be the maximal for fluid velocities slightly higher than the slow-particle velocity. In order to ensure the generalization of our conclusions beyond the details of our model, we have performed additional simulations which show that the expulsion mechanism also occurs in mixtures of spherical particles, other swimming strategies like active Brownian particles, and in other confining geometries as the presence of obstacles. Qualitatively, the results are expected to persist in three dimensional structures, as is the case for a single swimmer in Poiseuille flow [23].

Our results should be of considerable theoretical and practical interest, because they provide new insights into active matter and non-equilibrium systems. Applications of these results can be envisioned for the development of multi-stage cascade microfluidic lab-on-chip devices, which could then be an alternative to the use of laser traps or other external fields, for sorting particles with different motilities.

We thank L. Angelani, R. Di Leonardo and A. Wysocki

for very useful discussions. A.C. acknowledges partial support by the International Helmholtz Research School of Biophysics and Soft Matter (IHRS BioSoft).

REFERENCES

- [1] VICSEK T. and ZAFEIRIS A., *Phys. Rep.*, **517** (2012) 71.
- [2] LAUGA E. and POWERS T. R., *Rep. Prog. Phys.*, **72** (2009) 096601.
- [3] YANG M. and RIPOLL M., *Phys. Rev. E*, **84** (2011) 061401.
- [4] YANG Y. *et al.*, *Phys. Rev. E*, **82** (2010) 031904.
- [5] WENSINK H. H. *et al.*, *Proc. Natl. Acad. Sci. U.S.A.*, **109** (2012) 14308.
- [6] FILY Y. and MARCHETTI M. C., *Phys. Rev. Lett.*, **108** (2012) 235702.
- [7] ABKENAR M., *et al.*, *Phys. Rev. E*, **88** (2013) 062314.
- [8] WYSOCKI A. *et al.*, *EPL*, **105** (2014) 48004.
- [9] BUTTINONI I. *et al.*, *Phys. Rev. Lett.*, **110** (2013) 238301.
- [10] THEURKAUFF I. *et al.*, *Phys. Rev. Lett.*, **108** (2012) 268303.
- [11] STENHAMMAR J. *et al.*, *Phys. Rev. Lett.*, **111** (2013) 145702.
- [12] GALAJDA P., *et al.*, *J. Bacteriol.*, **189** (2007) 8704.
- [13] TAILLEUR J. and CATES M. E., *EPL*, **86** (2009) 60002.
- [14] ELGETI J. and GOMPPER G., *EPL*, **85** (2009) 38002.
- [15] ELGETI J. and GOMPPER G., *EPL*, **101** (2013) 48003.
- [16] WENSINK H. and LÖWEN H., *Phys. Rev. E*, **78** (2008) 031409.
- [17] KAISER A., *et al.*, *Phys. Rev. Lett.*, **108** (2012) 268307.
- [18] KAISER A., *et al.*, *Phys. Rev. E*, **88** (2013) 022311.
- [19] WIOLAND H. *et al.*, *Phys. Rev. Lett.*, **110** (2013) 268102.
- [20] RUSCONI R. *et al.*, *Nature Physics*, **10** (2014) 212.
- [21] COSTANZO A. *et al.*, *J. Phys.: Condens. Matter*, **24** (2012) 065101.
- [22] ZÖTTL A. and STARK H., *Phys. Rev. Lett.*, **108** (2012) 218104.
- [23] ZÖTTL A. and STARK H., *Eur. Phys. J. E*, **36** (2013) 4.
- [24] HILL J. *et al.*, *Phys. Rev. Lett.*, **98** (2007) 068101.
- [25] ANGELANI L. *et al.*, *Phys. Rev. Lett.*, **102** (2009) 048104.
- [26] DI LEONARDO R. *et al.*, *Proc. Natl. Acad. Sci. USA*, **107** (2010) 9541.
- [27] SOKOLOV A. *et al.*, *Proc. Natl. Acad. Sci. USA*, **107** (2010) 969.
- [28] ANGELANI L. *et al.*, *EPL*, **96** (2011) 68002.
- [29] GHOSH P. K. *et al.*, *Phys. Rev. Lett.*, **110** (2013) 268301.
- [30] POTOTSKY A. *et al.*, *Phys. Rev. E*, **87** (2013) 042124.
- [31] REGUERA D. *et al.*, *Phys. Rev. Lett.*, **108** (2012) 020604.
- [32] HONG D. C. *et al.*, *Phys. Rev. Lett.*, **86** (2001) 3423.
- [33] BRODY J. P. and YAGER P., *Sens. Actuat. A-Phys.*, **58** (1997) 13.
- [34] DUKE T. and AUSTIN R., *Phys. Rev. Lett.*, **80** (1998) 1552.
- [35] LOUTHERBACK K. *et al.*, *Phys. Rev. Lett.*, **102** (2009) 045301.
- [36] VOLPE G. *et al.*, *Soft Matter*, **7** (2011) 8810.
- [37] MIJALKOV M. and VOLPE G., *Soft Matter*, **9** (2013) 6376.
- [38] MCCANDLISH S. R. *et al.*, *Soft Matter*, **8** (2012) 2527.
- [39] BERDAKIN I., *et al.*, *Phys. Rev. E*, **87** (2013) 052702.
- [40] MAGGI C. *et al.*, *Soft Matter*, **9** (2013) 10885.
- [41] BERG H. C., *E. Coli in Motion* (Springer) 2004.

- [42] DRESCHER K. *et al.*, *Proc. Natl. Acad. Sci. USA*, **108**
(2011) 10940